30. Zherlitsyn, A.G. et al., Generation of intense microsecond-length microwave pulses in a virtual-cathode triode, *Sov. Tech. Phys. Lett.*, 11, 450, 1985.
31. Coleman, P.D. and Aurand, V.F., Long pulse virtual cathode oscillator experiments, in *Proceedings of the 1988 IEEE International Conference on Plasma Science*, Seattle, WA, 1988, p. 99.
32. Huttlin, G. et al., Reflex-diode HPM source on Aurora, *IEEE Trans. Plasma Sci.*, 18, 618, 1990, and references therein.
33. Davis, H. et al., Experimental confirmation of the reditron concept, *IEEE Trans. Plasma Sci.*, 16, 192, 1988; Davis, H., Enhanced-efficiency, narrow-band gigawatt microwave output of the reditron oscillator, *IEEE Trans. Plasma Sci.*, 18, 611, 1990.
34. Kwan, T.J. and Davis, H.A., Numerical simulations of the reditron, *IEEE Trans. Plasma Sci.*, 16, 185, 1988.
35. Kwan, T. et al., Beam bunch production and microwave generation in reditrons, *Proc. SPIE*, 1061, 100, 1989.
36. Madonna, R. and Scheno, P., Frequency stabilization of a vircator by use of a slow-wave structure, in *Proceedings of the 1990 IEEE International Conference on Plasma Science*, Oakland, CA, 1990, p. 133.
37. Zherlitsin, A., Melnikov, G., and Fomenko, G., Experimental investigation of the intense electron beam modulation by virtual cathode, in *Proceedings of BEAMS'88*, Karlsruhe, Germany, 1988, p. 1413.
38. Sze, H., Price, D., and Harteneck, B., Phase locking of two strongly coupled vircators, *J. Appl. Phys.*, 67, 2278, 1990.
39. Fazio, M., Hoeberling, R., and Kenross-Wright, J., Narrow-band microwave generation from an oscillating virtual cathode in a resonant cavity, *J. Appl. Phys.*, 65, 1321, 1989.
40. Gadestski, P. et al., The virtode: a generator using supercritical REB current with controlled feedback, *Plasma Phys. Rep.*, 19, 273, 1993.
41. Kitsanov, S.A. et al., S-band vircator with electron beam premodulation based on compact pulse driver with inductive energy storage, *IEEE Trans. Plasma Sci.*, 30, 1179, 2002.
42. Jiang, W. et al., High-power microwave generation by a coaxial virtual cathode oscillator, *IEEE Trans. Plasma Sci.*, 27, 1538, 1999.
43. Jiang, W., Dickens, J., and Kristiansen, M., Efficiency enhancement of a coaxial virtual cathode oscillator, *IEEE Trans. Plasma Sci.*, 27, 1543, 1999.
44. Didenko, A. et al., Investigation of wave electromagnetic generation mechanism in the virtual cathode system, in *Proceedings of BEAMS'88*, Karlsruhe, Germany, 1988, p. 1402.
45. Price, D. and Sze, H., Phase-stability analysis of the magnetron-driven vircator experiment, *IEEE Trans. Plasma Sci.*, 18, 580, 1990.
46. See Dumbrajs, O. and Nusinovich, G.S., Coaxial gyrotrons: past, present, and future (a review), *IEEE Trans. Plasma Sci.*, 32, 934, 2004, and the references therein.
47. Flyagin, V.A. et al., The gyrotron, *IEEE Trans. Microwave Theory Tech.*, MTT-25, 514, 1977.
48. Hirshfield, J.L. and Granatstein, V.L., The electron cyclotron maser: an historical survey, *IEEE Trans. Microwave Theory Tech.*, MTT-25, 522, 1977.

49. Twiss, R.Q., Radiation transfer and the possibility of negative absorption in radio astronomy, *Aust. J. Phys.*, 11, 564, 1958; Twiss, R.Q. and Roberts, J.A., Electromagnetic radiation from electrons rotating in an ionized medium under the action of a uniform magnetic field, *Aust. J. Phys.*, 11, 424, 1958.
50. Schneider, J., Stimulated emission of radiation by relativistic electrons in a magnetic field, *Phys. Rev. Lett.*, 2, 504, 1959.
51. Gaponov, A.V., Addendum, *Izv. VUZ Radiofiz.*, 2, 837, 1959; an addendum to Gaponov, A.V., Interaction between electron fluxes and electromagnetic waves in waveguides, *Izv. VUZ Radiofiz.*, 2, 450, 1959.
52. Hirshfeld, J.L. and Wachtel, J.M., Electron cyclotron maser, *Phys. Rev. Lett.*, 12, 533, 1964.
53. Gaponov, A.V., Petelin, M.I., and Yulpatov, V.K., The induced radiation of excited classical oscillators and its use in high-frequency electronics, *Izv. VUZ Radiofiz.*, 10, 1414, 1967 (*Radiophys. Quantum Electron.*, 10, 794, 1967).
54. Baird, J.M., Gyrotron theory, in *High-Power Microwave Sources*, Granatstein, V.L. and Alexeff, I., Eds., Artech House, Norwood, MA, 1987, p. 103.
55. Gaponov, A.V. et al., Some perspectives on the use of powerful gyrotrons for the electron-cyclotron plasma heating in large tokamaks, *Int. J. Infrared Millimeter Waves*, 1, 351, 1980.
56. See Gaponov, A.V. et al., Experimental investigation of centimeter-band gyrotrons, *Izv. VUZ Radiofiz.*, 18, 280, 1975 (*Radiophys. Quantum Electron.*, 18, 204, 1975).
57. Kisel, D.V. et al., An experimental study of a gyrotron, operating in the second harmonic of the cyclotron frequency, with optimized distribution of the high-frequency field, *Radio Eng. Electron Phys.*, 19, 95, 1974.
58. Litvak, A.G. et al., Gyrotrons for Fusion. Status and Prospects, paper presented at the 18th IAEA Fusion Energy Conference, Sorrento, Italy, 2000 (published online, available from http://www-naweb.iaea.org/napc/physics/ps/conf.htm).
59. Granatstein, V.L. et al., Gigawatt microwave emission from an intense relativistic electron beam, *Plasma Phys.*, 17, 23, 1975.
60. Lawson, W. et al., High-power operation of a three-cavity X-band coaxial gyroklystron, *Phys. Rev. Lett.*, 81, 3030, 1998.
61. Botvinnik, I.E. et al., Free electron masers with Bragg resonators, *Pis'ma Zh. Eksp. Teor. Fiz.*, 35, 418, 1982 (*JETP Lett.*, 35, 516, 1982).
62. Botvinnik, I.E. et al., Cyclotron-autoresonance maser with a wavelength of 2.4 mm, *Pis'ma Zh. Tekh. Fiz.*, 8, 1386, 1982 (*Sov. Tech. Phys. Lett.*, 8, 596, 1982).
63. Rapoport, G.N., Nemak, A.K., and Zhurakhovskiy, V.A., Interaction between helical electron beams and strong electromagnetic cavity-fields at cyclotron-frequency harmonics, *Radioteck. Elektron.*, 12, 633, 1967 (*Radio Eng. Electron. Phys.*, 12, 587, 1967).
64. Sprangle, P., Vomvoridis, J.L., and Manheimer, W.M., Theory of the quasioptical electron cyclotron maser, *Phys. Rev. A*, 223, 3127, 1981.
65. Nezhevenko, O.A., Gyrocons and magnicons: microwave generators with circular deflection of the electron beam, *IEEE Trans. Plasma Sci.*, 22, 756, 1994.
66. Budker, G.I. et al., The gyrocon: an efficient relativistic high-power VHF generator, *Part. Accel.*, 10, 41, 1979.
67. Bratman, V.L. et al., Millimeter-wave HF relativistic electron oscillators, *IEEE Trans. Plasma Sci.*, PS-15, 2, 1987.

68. Sprangle, P. and Drobot, A.T., The linear and self-consistent nonlinear theory of the electron cyclotron maser instability, *IEEE Trans. Microwave Theory Tech.*, MTT-25, 528, 1977.
69. For a simplified analytical treatment, see Lentini, P.J., *Analytic Theory of the Gyrotron*, PFC/RR-89-6, Plasma Fusion Center, MIT, Cambridge, MA, 1989.
70. Nusinovich, G.S. and Erm, R.E., Efficiency of the CRM-monotron with a Gaussian axial structure of the high-frequency field, *Elektronnaya Technika, Elektronika SVCh*, 8, 55, 1972 (in Russian). Recounted in Nusinovich, G.S., *Introduction to the Physics of Gyrotrons*, Johns Hopkins University Press, Baltimore, MD, 2004, p. 74.
71. Bratman, V.L. et al., Relativistic gyrotrons and cyclotron autoresonance masers, *Int. J. Electron.*, 51, 541, 1981.
72. Danly, B.G. and Temkin, R.J., Generalized nonlinear harmonic gyrotron theory, *Phys. Fluids*, 29, 561, 1986.
73. Chu, K.R. and Hirshfeld, J.L., Comparative study of the axial and azimuthal bunching mechanisms in electromagnetic cyclotron instabilities, *Phys. Fluids*, 21, 461, 1978.
74. As an example, see Kho, T.H. and Lin, A.T., Slow-wave electron cyclotron maser, *Phys. Rev. A*, 38, 2883, 1988.
75. Granatstein, V.L., Gyrotron experimental studies, in *High-Power Microwave Sources*, Granatstein, V.L. and Alexeff, I., Eds., Artech House, Norwood, MA, 1987, p. 185.
76. Temkin, R.J. et al., A 100 kW, 140 GHz pulsed gyrotron, *Int. J. Infrared Millimeter Waves*, 3, 427, 1982.
77. Carmel, Y. et al., Mode competition, suppression, and efficiency enhancement in overmoded gyrotron oscillators, *Int. J. Infrared Millimeter Waves*, 3, 645, 1982.
78. Arfin, B. et al., A high power gyrotron operating in the TE_{041} mode, *IEEE Trans. Electron. Dev.*, ED-29, 1911, 1982.
79. See, for example, Carmel, Y. et al., Realization of a stable and highly efficient gyrotron for controlled fusion research, *Phys. Rev. Lett.*, 50, 1121, 1983.
80. See, for example, Luchinin, A.G. and Nusinovich, G.S., An analytical theory for comparing the efficiency of gyrotrons with various electrodynamic systems, *Int. J. Electron.*, 57, 827, 1984.
81. Anderson, J.P. et al., Studies of the 1.5-MW 140-GHz gyrotron experiment, *IEEE Trans. Plasma Sci.*, 32, 877, 2004.
82. Pioszcyk, B. et al., 165-GHz coaxial cavity gyrotron, *IEEE Trans. Plasma Sci.*, 32, 853, 2004.
83. Kreischer, K.E. et al., The design of megawatt gyrotrons, *IEEE Trans. Plasma Sci.*, PS-13, 364, 1985.
84. Danly, B.G. et al., Whispering-gallery-mode gyrotron operation with a quasi-optical antenna, *IEEE Trans. Plasma Sci.*, PS-13, 383, 1985.
85. Flyagin, V.A. and Nusinovich, G.S., Gyrotron oscillators, *Proc. IEEE*, 76, 644, 1988.
86. Chu, K.R., Read, M.E., and Ganguly, A.K., Methods of efficiency enhancement and scaling for the gyrotron oscillator, *IEEE Trans. Microwave Theory Tech.*, MTT-28, 318, 1980.
87. Felch, K. et al., Long-pulse and CW tests of a 110-GHz gyrotron with an internal, quasi-optical converter, *IEEE Trans. Plasma Sci.*, 24, 558, 1996.
88. Blank, M. et al., Demonstration of a high-power long-pulse 140-GHz gyrotron oscillator, *IEEE Trans. Plasma Sci.*, 32, 867, 2004.
89. Gold, S.H. et al., High-voltage K_a-band gyrotron experiment, *IEEE Trans. Plasma Sci.*, PS-13, 374, 1985.
90. Gold, S.H. et al., High peak power K_a-band gyrotron oscillator experiment, *Phys. Fluids*, 30, 2226, 1987.
91. Gold, S.H., High peak power K_a-band gyrotron oscillator experiments with slotted and unslotted cavities, *IEEE Trans. Plasma Sci.*, 16, 142, 1988.
92. Black, W.M. et al., Megavolt multikiloamp K_a band gyrotron oscillator experiment, *Phys. Fluids B*, 2, 193, 1990.
93. Kreischer, K.E. and Temkin, R.J., Single-mode operation of a high-power, step-tunable gyrotron, *Phys. Rev. Lett.*, 59, 547, 1987.
94. Davidovskii, V.Ya., Possibility of resonance acceleration of charged particles by electromagnetic waves in a constant magnetic field, *Zh. Eksp. Teor. Fiz.*, 43, 886, 1962 (*Sov. Phys. JETP*, 16, 629, 1963).
95. Kolomenskii, A.A. and Lebedev, A.N., Self-resonant particle motion in a plane electromagnetic wave, *Dokl. Akad Nauk SSSR*, 149, 1259, 1962 (*Sov. Phys. Dokl.*, 7, 745, 1963).
96. Bratman, V.L. et al., FELs with Bragg reflection resonators: cyclotron autoresonance masers versus ubitrons, *IEEE J. Quantum Electron.*, QE-19, 282, 1983.
97. Yovchev, I.G. et al., Present status of a 17.1-GHz four-cavity frequency-doubling coaxial gyroklystron design, *IEEE Trans. Plasma Sci.*, 28, 523, 2000.
98. Lawson, W., On the frequency scaling of coaxial gyroklystrons, *IEEE Trans. Plasma Sci.*, 30, 876, 2002.
99. Lawson, W., Ragnunathan, H., and Esteban, M., Space-charge-limited magnetron injection guns for high-power gyrotrons, *IEEE Trans. Plasma Sci.*, 32, 1236, 2004.
100. McCurdy, A.H. et al., Improved oscillator phase locking by use of a modulated electron beam in a gyrotron, *Phys. Rev. Lett.*, 57, 2379, 1986.
101. Freund, H. and Antonsen, T.M., *Principles of Free-Electron Lasers*, 2nd ed., Chapman & Hall, London, 1996.
102. Kapitsa, P.L. and Dirac, P.A.M., *Proc. Cambr. Phil. Soc.*, 29, 247, 1933.
103. Motz, H., Applications of the radiation from fast electrons, *J. Appl. Phys.*, 22, 257, 1951.
104. Phillips, R.M., The ubitron, a high-power traveling-wave tube based on a periodic beam interaction in an unloaded waveguide, *IRE Trans. Electron. Dev.*, ED-7, 231, 1960; Phillips, R.M., History of the ubitron, *Nucl. Instrum. Methods*, A272, 1, 1988.
105. Madey, J.M.J., Stimulated emission of bremsstrahlung in a periodic magnetic field, *J. Appl. Phys.*, 42, 1906, 1971.
106. Elias, L.R. et al., Observation of stimulated emission of radiation by relativistic electrons in a spatially periodic transverse magnetic field, *Phys. Rev. Lett.*, 36, 717, 1976.
107. Deacon, D.A.G. et al., First operation of a free-electron laser, *Phys. Rev. Lett.*, 38, 892, 1977.
108. Kroll, N.M., Morton, P., and Rosenbluth, M.N., Free-electron lasers with variable parameter wigglers, *IEEE J. Quantum Electron.*, QE-17, 1436, 1981.
109. See, for example, Fajans, J. et al., Microwave studies of a tunable free-electron laser in combined axial and wiggler magnetic fields, *Phys. Fluids*, 26, 2683, 1983.
110. Gold, S.H. et al., Study of gain, bandwidth, and tunability of a millimeter-wave free-electron laser operating in the collective regime, *Phys. Fluids*, 26, 2683, 1983.

111. Latham, P.E. and Levush, B., The interaction of high- and low-frequency waves in a free electron laser, *IEEE Trans. Plasma Sci.*, 18, 472, 1990.
112. Instabilities can be convective and absolute, a subject beyond our scope here, but the classic treatment is Briggs, R.J., *Electron Stream Interaction with Plasma*, MIT Press, Cambridge, MA, 1964, chap. 2.
113. Liewer, P.C., Lin, A.T., and Dawson, J.M., Theory of an absolute instability of a finite-length free-electron laser, *Phys. Rev. A*, 23, 1251, 1981.
114. Kwan, T.J.T., Application of particle-in-cell simulation in free-electron lasers, *IEEE J. Quantum Electron.*, QE-17, 1394, 1981.
115. Kroll, N.M. and McMullin, W.A., Stimulated emission from relativistic electron passing through a spatially periodic transverse magnetic field, *Phys. Rev. A*, 17, 300, 1978; Sprangle, P. and Smith, R.A., Theory of free-electron lasers, *Phys. Rev. A*, 21, 293, 1980.
116. Friedland, L., Electron beam dynamics in combined guide and pump magnetic fields for free electron laser applications, *Phys. Fluids*, 23, 2376, 1980; Freund, H.P. and Drobot, A.T., Relativistic electron trajectories in free electron lasers with an axial guide field, *Phys. Fluids*, 25, 736, 1982; Freund, H.P. and Ganguly, A.K., Electron orbits in free-electron lasers with helical wiggler and an axial guide magnetic field, *IEEE J. Quantum Electron.*, QE-21, 1073, 1985.
117. Jackson, R.H. et al., Design and operation of a collective millimeter-wave free-electron laser, *IEEE J. Quantum Electron.*, QE-19, 346, 1983.
118. Freund, H.P. et al., Collective effects on the operation of free-electron lasers with an axial guide field, *Phys. Rev. A*, 26, 2004, 1982; Freund, H.P. and Sprangle, P., Unstable electrostatic beam modes in free-electron-laser systems, *Phys. Rev. A*, 28, 1835, 1983.
119. Parker, R.K. et al., Axial magnetic-field effects in a collective-interaction free-electron laser at millimeter wavelengths, *Phys. Rev. Lett.*, 48, 238, 1982.
120. Conde, M.E., Bekefi, G., and Wurtele, J.S., A 33 GHz free electron laser with reversed axial guide magnetic field, in *Abstracts for the 1991 IEEE International Conference on Plasma Science*, Williamsburg, VA, 1991, p. 176.
121. Pasour, J.A., Free-electron lasers, in *High-Power Microwave Sources*, Granatstein, V.L. and Alexeff, I., Eds., Artech House, Norwood, MA, 1987.
122. Orzechowski, T.J. et al., High gain and high extraction efficiency from a free electron laser amplifier operating in the millimeter wave regime, *Nucl. Instrum. Methods*, A250, 144, 1986.
123. Freund, H.P. and Ganguly, A.K., Nonlinear analysis of efficiency enhancement in free-electron laser amplifiers, *Phys. Rev. A*, 33, 1060, 1986.
124. Kroll, N.M. and Rosenbluth, M.N., *Physics of Quantum Elecronics*, Vol. 7, Jacobs, S.F. et al., Eds., Addison-Wesley, Reading, MA, 1980, p. 147.
125. Colson, W.B. and Freedman, R.A., Synchrotron instability for long pulses in free electron laser oscillator, *Opt. Commun.*, 46, 37, 1983.
126. Colson, W.B., The trapped-particle instability in free electron laser oscillators and amplifiers, *Nucl. Instrum. Methods*, A250, 168, 1986.
127. Masud, J. et al., Sideband control in a millimeter-wave free-electron laser, *Phys. Rev. Lett.*, 58, 763, 1987.
128. Yu, S.S. et al., Waveguide suppression of the free electron laser sideband instability, *Nucl. Instrum. Methods*, 259, 219, 1987.
129. Yee, F.G. et al., Power and sideband studies of a Raman FEL, *Nucl. Instrum. Methods*, A259, 104, 1987.
130. Throop, A.L. et al., Experimental Characteristic of a High-Gain Free-Electron Laser Amplifier Operating at 8-mm and 2-mm Wavelengths, UCRL-95670, Lawrence Livermore National Laboratory, Livermore, CA, 1987.
131. Hester, R.E. et al., The Experimental Test Accelerator (ETA), *IEEE Trans. Nucl. Sci.*, NS-26, 3, 1979.
132. Orzechowski, T.J. et al., High-efficiency extraction of microwave radiation from a tapered-wiggler free-electron laser, *Phys. Rev. Lett.*, 57, 2172, 1986.
133. Allen, S.L. et al., Generation of high power 140 GHz microwaves with an FEL for the MTX experiment, in *Proceedings of the 1993 Particle Accelerator Conference*, Washington, D.C., 1993, p. 1551.
134. Lasnier, C.J. et al., Burst mode FEL with the ETA-III induction linac, in *Proceedings of the 1993 Particle Accelerator Conference*, Washington, D.C., 1993, p. 1554.
135. Vinokurov, N.A. and Skrinskiy, A.N., Institute of Nuclear Physics Preprint INP 11-59, Novosibirsk, 1977.
136. Leibovitch, C., Xu, K., and Bekefi, G., Effects of electron prebunching on the radiation growth rate of a collective (Raman) free-electron laser amplifier, *IEEE J. Quantum Electron.*, 24, 1825, 1988.
137. Wurtele, J.S. et al., Prebunching in a collective Raman free-electron laser amplifier, *Phys. Fluids B*, 2, 402, 1990.
138. Fajans, J. and Wurtele, J.S., Suppression of feedback oscillations in a free-electron laser, *IEEE J. Quantum Electron.*, 24, 1805, 1990.
139. Agafonov, M.A. et al., Generation of hundred joules pulses at 4-mm wavelength by FEM with sheet electron beam, *IEEE Trans. Plasma Sci.*, 26, 531, 1998.

Appendix

High Power Microwave Formulary

For plasma physics and much else, see the NRL Plasma Formulary, http://www.ppd.nrl.navy.mil/nrlformulary/. Much microwave information appears in *Microwave Engineers' Handbook*, Volumes 1 and 2, Artech House, Norwood, MA.

A.1 Electromagnetism

- *Definitions of Q*:

1. $$Q = 2\pi \frac{\text{average stored energy}}{\text{energy lost per cycle}} = \omega_0 \frac{\text{average stored energy}}{\text{power loss rate}}$$

ω_0 is the center frequency of a cavity of resonant line width $\Delta\omega$,

2. $$Q = \frac{\omega_0}{2\Delta\omega}$$

3. $$Q_p = \frac{\text{cavity volume}}{(\text{surface area}) \times \delta} \times (\text{geometrical factor})$$

The geometrical factor is typically of order unity.

4. The number of cycles in a pulse, the bandwidth, and the Q of the resonant system that produces a pulse are related by

$$\text{N} = 1/\text{percentage bandwidth} = \text{Q}$$

5. The radiated energy loss time constant from the cavity T_r, as the ratio of the stored energy to the power lost from the cavity, is

$$Q_r = \omega_0 T_r$$

6. If the cavity has highly reflecting ends with reflection coefficients R_1 and R_2, then

$$T_r \approx \frac{L}{v_g\left(1 - R_1 R_2\right)}$$

- *Skin depth*:

$$\delta = \frac{1}{\left(\pi\sigma\mu w_f\right)^{1/2}} = \frac{1}{\left(\pi\sigma\mu_0 f\right)^{1/2}}$$

In copper, $\sigma = 5.80 \times 10^7$ $(\Omega\text{-m})^{-1}$; skin depth at 1 GHz is 2.1 μm.

TABLE A.1

Conductivities of Some Materials

Material	Conductivity $(\Omega\text{-m})^{-1}$
Aluminum	3.82×10^7
Brass	2.6×10^7
Copper	5.8×10^7
Gold	4.1×10^7
Graphite	7×10^4
Iron	1.03×10^7
Lead	4.6×10^6
Sea water	3–5
Silver	6.2×10^7
Stainless steel	1.1×10^6

A.2 Waveguides and Cavities

TABLE A.2

Expressions for the TM and TE Field Quantities for a Rectangular Waveguide in Terms of the Axial Field Component, Derived from Equations 4.1 to 4.4

Transverse Magnetic, $TM_{n,p}$	Transverse Electric, $TE_{n,p}$
$E_z = D\sin\left(\frac{n\pi}{a}x\right)\sin\left(\frac{p\pi}{b}y\right)$	$B_z = A\cos\left(\frac{n\pi}{a}x\right)\cos\left(\frac{p\pi}{b}y\right)$
$B_z \equiv 0$	$E_z \equiv 0$
$E_x = i\frac{k_z}{k_\perp^2}\frac{\partial E_z}{\partial x}$	$E_x = i\frac{\omega}{k_\perp^2}\frac{\partial B_z}{\partial y}$
$E_y = -i\frac{k_z}{k_\perp^2}\frac{\partial E_z}{\partial y}$	$E_y = -i\frac{\omega}{k_\perp^2}\frac{\partial B_z}{\partial x}$
$B_x = -i\frac{\omega}{\omega_{co}^2}\frac{\partial E_z}{\partial y}$	$B_x = i\frac{k_z}{k_\perp^2}\frac{\partial B_z}{\partial x}$
$B_y = i\frac{\omega}{\omega_{co}^2}\frac{\partial E_z}{\partial x}$	$B_y = i\frac{k_z}{k_\perp^2}\frac{\partial B_z}{\partial y}$
$\omega_{co} = k_\perp c = \left[\left(\frac{n\pi c}{a}\right)^2 + \left(\frac{p\pi c}{b}\right)^2\right]^{1/2}$	

TABLE A.3

Cutoff Frequencies, Measured in GHz, for the Lowest-Order Modes of WR284 Waveguide

n	p	$f_{co} = \omega_{co}/2\pi$ (GHz) a = 7.214 cm, b = 3.404 cm
1	0	2.079
0	1	4.407
1	1	4.873
1	2	9.055
2	0	4.159
2	1	6.059

TABLE A.4

Expressions for the TM and TE Field Quantities for Circular Waveguide in Terms of the Axial Field Components, Derived from Equations 4.1 to 4.4

Transverse Magnetic, $TM_{n,p}$ ($B_z = 0$)	Transverse Electric, $TE_{n,p}$ ($E_z = 0$)
$E_z = DJ_p(k_\perp r)\sin(p\theta)$	$B_z = AJ_p(k_\perp r)\sin(p\theta)$
$E_r = i\frac{k_z}{k_\perp^2}\frac{\partial E_z}{\partial r}$	$E_r = i\frac{\omega}{k_\perp^2}\frac{1}{r}\frac{\partial B_z}{\partial \theta}$
$E_\theta = i\frac{k_z}{k_\perp^2}\frac{1}{r}\frac{\partial E_z}{\partial \theta}$	$E_\theta = -i\frac{\omega}{k_\perp^2}\frac{\partial B_z}{\partial r}$
$B_r = -i\frac{\omega}{\omega_{co}^2}\frac{1}{r}\frac{\partial E_z}{\partial \theta}$	$B_r = i\frac{k_z}{k_\perp^2}\frac{\partial B_z}{\partial r}$
$B_\theta = i\frac{\omega}{\omega_{co}^2}\frac{\partial E_z}{\partial r}$	$B_\theta = i\frac{k_z}{k_\perp^2}\frac{1}{r}\frac{\partial B_z}{\partial \theta}$
$k_\perp = \frac{\omega_{co}}{c} = \frac{\mu_{pn}}{r_0}$	$k_\perp = \frac{\omega_{co}}{c} = \frac{\nu_{pn}}{r_0}$
$J_p(\mu_{pn}) = 0$	$J_p'(\nu_{pn}) = 0$

TABLE A.5

Relationship between the Power in a Given Mode, P, and the Maximum Value of the Electric Field at the Wall, $E_{wall,max}$

Mode	
Rectangular	
TM	$P_{TM} = \frac{ab}{8Z_0}\left[\left(\frac{n}{a}\right)^2+\left(\frac{p}{b}\right)^2\right]\frac{1}{\left[1-\left(\frac{f_{co}}{f}\right)^2\right]^{1/2}}\min\left[\left(\frac{a}{n}\right)^2,\left(\frac{b}{p}\right)^2\right]E_{wall,max}^2$
TE n, p > 0	$P_{TE} = \frac{ab}{8Z_0}\left[\left(\frac{n}{a}\right)^2+\left(\frac{p}{b}\right)^2\right]\left[1-\left(\frac{f_{co}}{f}\right)^2\right]^{1/2}\min\left[\left(\frac{a}{n}\right)^2,\left(\frac{b}{p}\right)^2\right]E_{wall,max}^2$
TE n or p = 0	$P_{TE} = \frac{ab}{4Z_0}\left[\left(\frac{n}{a}\right)^2+\left(\frac{p}{b}\right)^2\right]\left[1-\left(\frac{f_{co}}{f}\right)^2\right]^{1/2}\min\left[\left(\frac{a}{n}\right)^2,\left(\frac{b}{p}\right)^2\right]E_{wall,max}^2$

Continued.

TABLE A.5 *(Continued)*

Relationship between the Power in a Given Mode, P, and the Maximum Value of the Electric Field at the Wall, $E_{wall,max}$

Mode	
Circular	
TM	$P_{TM} = \frac{\pi r_0^2}{4Z_0}\frac{E_{wall,max}^2}{\left[1-\left(\frac{f_{co}}{f}\right)^2\right]^{1/2}}$
TE p > 0	$P_{TE} = \frac{\pi r_0^2}{2Z_0}\left[1-\left(\frac{f_{co}}{f}\right)^2\right]^{1/2}\left[1+\left(\frac{\nu_{pn}^2}{p}\right)^2\right]E_{wall,max}^2$

Note: Min(x, y) is the smaller of x and y, and $Z_0 = 377\ \Omega$.

TABLE A.6

Standard Rectangular Waveguides

Band (Alternate)	Recommended Frequency Range (GHz)	TE_{10} Cutoff Frequency (GHz)	WR Number	Inside Dimensions, Inches (cm)
L	1.12–1.70	0.908	650	6.50 × 3.25 (16.51 × 8.26)
R	1.70–2.60	1.372	430	4.30 × 2.15 (10.92 × 5.46)
S	2.60–3.95	2.078	284	2.84 × 1.34 (7.21 × 3.40)
H (G)	3.95–5.85	3.152	187	1.87 × 0.87 (4.76 × 2.22)
C (J)	5.85–8.20	4.301	137	1.37 × 0.62 (3.49 × 1.58)
W (H)	7.05–10.0	5.259	112	1.12 × 0.50 (2.85 × 1.26)
X	8.20–12.4	6.557	90	0.90 × 0.40 (2.29 × 1.02)
Ku (P)	12.4–18.0	9.486	62	0.62 × 0.31 (1.58 × 0.79)
K	18.0–26.5	14.047	42	0.42 × 0.17 (1.07 × 0.43)
Ka (R)	26.5–40.0	21.081	28	0.28 × 0.14 (0.71 × 0.36)
Q	33.0–50.5	26.342	22	0.22 × 0.11 (0.57 × 0.28)
U	40.0–60.0	31.357	19	0.19 × 0.09 (0.48 × 0.24)

Continued.

TABLE A.6 *(Continued)*

Standard Rectangular Waveguides

Band (Alternate)	Recommended Frequency Range (GHz)	TE_{10} Cutoff Frequency (GHz)	WR Number	Inside Dimensions, Inches (cm)
V	50.0–75.0	39.863	15	0.15 × 0.07 (0.38 × 0.19)
E	60.0–90.0	48.350	12	0.12 × 0.06 (0.31 × 0.02)
W	75.0–110.0	59.010	10	0.10 × 0.05 (0.25 × 0.13)
F	90.0–140.0	73.840	8	0.08 × 0.04 (0.20 × 0.10)
D	110.0–170.0	90.854	6	0.07 × 0.03 (0.17 × 0.08)
G	140.0–220.0	115.750	5	0.05 × 0.03 (0.13 × 0.06)

A.3 Pulsed Power and Beams

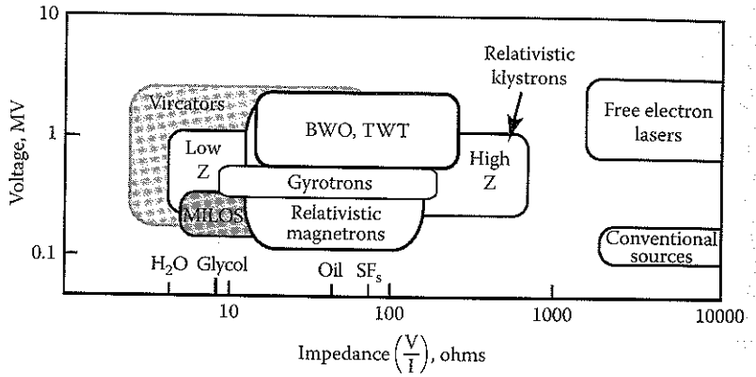

FIGURE A.1
Voltage and impedance of parameter space for HPM and pulsed conventional sources and optimum impedances for widely used pulse line insulators (water, glycol, oil, SF_6).

- Below are optimum impedances of pulse-forming lines, maximizing energy density:
  - Oil line, 42 Ω
  - Ethylene glycol line, 9.7 Ω
  - Water line, 6.7 Ω

- On the other hand, liquid energy density is largest for water (0.9 relative to mylar), intermediate for glycol (0.45), and lowest for oil (0.06).

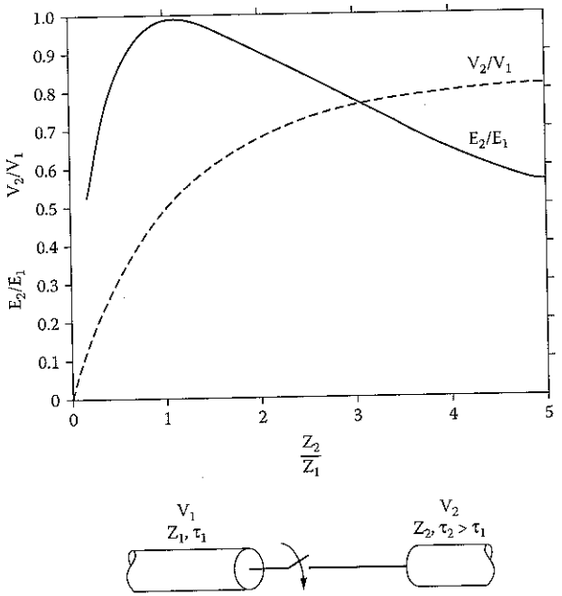

FIGURE A.2
Energy transfer and voltage ratios between transmission line (1) and load (2) as a function of impedance ratio.

Diodes and Beams

- Child–Langmuir current density, impedance:

$$J_{SCL}\left(\frac{kA}{cm^2}\right) = 2.33\frac{\left[V_0\left(MV\right)\right]^{3/2}}{\left[d\left(cm\right)\right]^2}$$

$$I_{SCL}\left(kA\right) = J_{SCL}A = 7.35\left[V_0\left(MV\right)\right]^{3/2}\left[\frac{r_c(cm)}{d(cm)}\right]^2$$

$$Z_{SCL}(\Omega) = \frac{136}{\sqrt{V_0\left(MV\right)}}\left[\frac{d}{r_c}\right]^2$$

- Relativistic Child–Langmuir current density:

$$J\left(\frac{\text{kA}}{\text{cm}^2}\right)=\frac{2.71}{\left[d(\text{cm})\right]^2}\left[\left(1+\frac{V_0(MV)}{0.511}\right)^{1/2}-0.847\right]^2$$

- Diode pinch current:

$$I_{\text{pinch}}(\text{kA})=8.5\frac{r_c}{d}\left[1+\left(\frac{V_0(\text{MV})}{0.511}\right)\right]$$

- Parapotential current, impedance; magnetic insulation current I_z must exceed the parapotential current:

$$I_z > I_p(A)=8500\gamma G\ell n\left(\gamma+\sqrt{\gamma^2-1}\right)$$

where γ is a relativistic factor and G is a geometric factor.

$G=[\ell n(b/a)]^{-1}$, coaxial cylinders of inner and outer radii b and a and $G = W/2\pi d$, parallel plates of width W, gap d.

$Z_p = V/I_p \approx 52G^{-1}\ \Omega$ for voltages ~1 MV.

A.4 Microwave Sources

TABLE A.7

Classification of HPM Sources

	Slow Wave	Fast Wave
O-Type	Backward wave oscillator	Free-electron laser (ubitron)
	Traveling wave tube	Optical klystron
	Surface wave oscillator	Gyrotron
	Relativistic diffraction generator	Gyro-BWO
	Orotron	Gyro-TWT
	Flimatron	Cyclotron autoresonance maser
	Multiwave Cerenkov generator	Gyroklystron
	Dielectric Cerenkov maser	
	Plasma Cerenkov maser	
	Relativistic klystron	
M-Type	Relativistic magnetron	Rippled-field magnetron
	Cross-field amplifier	
	Magnetically insulated line oscillator	
Space-Charge	Vircator	
	Reflex triode	

TABLE A.8

General Features of HPM Sources

Source	Operating Frequency	Efficiency	Complexity	Level of Development
Magnetron	1–9 GHz, BW ~ 1%	10–30%	Low	High
O-type Cerenkov devices	3–60 GHz, somewhat tunable	10–50%	Medium to high	High
Vircator	0.5–35 GHz, wide BW (≲10%), tunable	~1% simple ~10% advanced	Low	Medium
Electron cyclotron masers	5–300 GHz for gyrotrons, higher for CARMs	30% typical	Medium	High for gyrotrons Low for CARMs
FEL	8 GHz and up, tunable	35%	High	Medium to high
Relativistic klystron	1–11 GHz	25–50%	Medium to high	Medium

- *Phase locking* condition, known as *Adler's relation*:

$$\Delta\omega \le \frac{\omega_0\rho}{Q}$$

ω_0 is the mean frequency of the two oscillators, which have the same Q. The injection ratio is

$$\rho = \left(\frac{P_i}{P_0}\right)^{1/2} = \frac{E_i}{E_0}$$

Subscripts i and 0 denote the injecting (or master) and receiving (or slave) oscillators. Phase locking occurs when the frequency difference between the two oscillators is sufficiently small. The timescale for locking is given by

$$\tau \sim \frac{Q}{2\rho\omega_0}$$

For $\rho \sim 1$, the locking range $\Delta\omega$ is maximized and the timescale for locking is minimized.

TABLE A.9

Ultrawideband Band Regions

Bands		Percent Bandwidth, 100 Δf/f	Bandwidth Ratio, 1 + Δf/f	Example
Narrowband		<1%	1.01	Orion (Figures 5.31 and 7.24)
Ultrawideband	Moderate band (mesoband)	1–100%	1.01–3	MATRIX (Figure 6.11)
	Ultramoderate band (subhyperband)	100–163%	3–10	H-Series (Figure 6.16)
	Hyperband	163–200%	>10	Jolt (Figure 6.17)

A.5 Propagation and Antennas

- *Power density*: Critical fluence for air breakdown for pulses longer than a microsecond:

$$S\left[\frac{MW}{cm^2}\right] = 1.5\rho^2(atm)$$

where S is microwave power density and ρ is the pressure in units of an atmosphere. This corresponds to a critical field of 24 kV/cm at atmospheric pressure. The field due to microwave power density is

$$E(V/cm) = 19.4\ [S(W/cm^2)]^{1/2}$$

$$S(W/cm^2)] = E^2(V/cm)/377$$

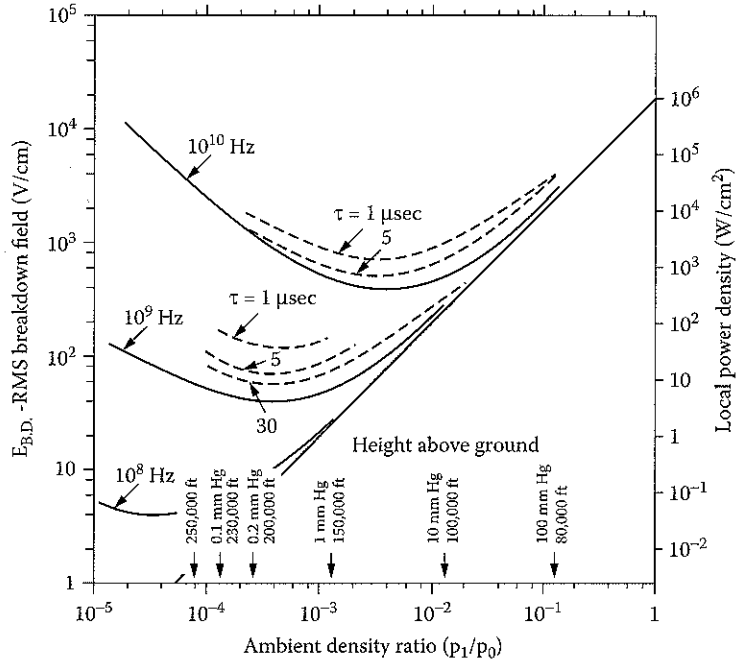

FIGURE A.3
Dependence of breakdown on pressure, frequency, and pulse duration.

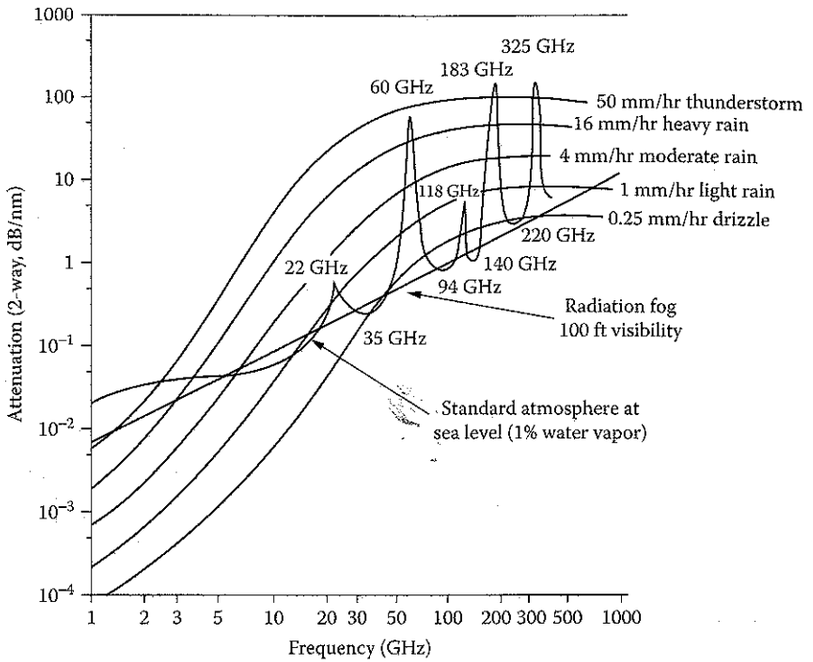

FIGURE A.4
Absorption in the air by water and oxygen molecules gives passbands at 35, 94, 140, and 220 GHz.

- *Directive gain*: The directive gain of an antenna is its ability to concentrate radiated power in a solid angle, Ω_A, producing a power density S at range R due to power P:

$$G_D = \frac{4\pi}{\Omega_A} = \frac{4\pi}{\Delta\theta\Delta\Phi} = \frac{4\pi R^2}{P} S$$

Beam widths in the two transverse dimensions are $\Delta\theta$ and $\Delta\phi$. The *gain*, G, is G_D times the antenna efficiency and can be expressed in terms of wavelength and area, $A = \pi D^2/4$:

$$G = G_D = \frac{4\pi A\varepsilon}{\lambda^2}$$

GP is the *effective radiated power* (ERP). The common way to describe gain is in decibels, G_{dB}. This value corresponds to an actual numerical value of

$$G = 10^{G_{dB}/10}$$

so a gain of 100 is called 20 dB.

The far field of a narrowband antenna begins at

$$L_{ff} = \frac{2D^2}{\lambda}$$

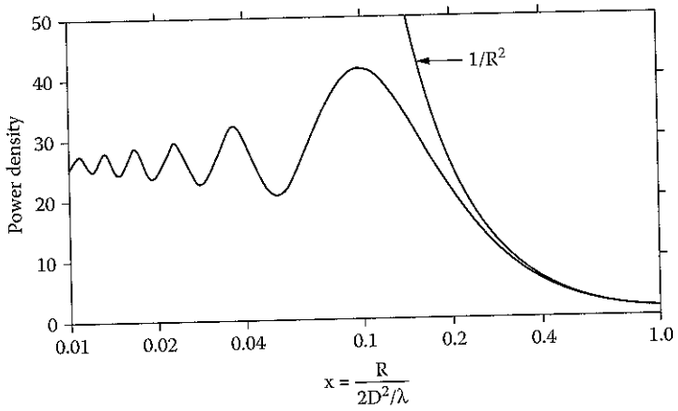

FIGURE A.5
Horn antenna intensity normalized to unity at $2D^2/\lambda$. Its general features are the same for most antenna types.

TABLE A.10

Principal Antenna Types

Antenna	Gain	Comments
Pyramidal and TEM horn	$2\pi ab/\lambda^2$	For standard gain horn; sides a, b; lengths $l_e = b^2/2\lambda$, $l_h = a^2/3\lambda$
Conical horn	$5\ D^2/\lambda^2$	$l = D^2/3\lambda$; D = diameter
Parabolic dish	$5.18\ D^2/\lambda^2$	
Vlasov	$6.36\ [D^2/\lambda^2]/\cos\theta$	Angle of slant-cut θ, $30° < \theta < 60°$
Biconic	$120\ \cot\alpha/4$	α is the bicone opening angle
Helical	$[148\ N\ S/\lambda]\ D^2/\lambda^2$	N = number of turns; S = spacing between turns
Array of horns	$9.4\ AB/\lambda^2$	A, B are sides of the array

The diffraction-limited beam width is

$$\theta = 2.44\ \lambda/D_t$$

This is the diffraction-limited divergence, giving the first null point of the Bessel function for a circular aperture and including 84% of the beam power. The size of this spot at range R is

$$D_s = \theta R = 2.44 \lambda R/D_t$$

A.6 Applications

Electronics effects power coupled to internal circuitry, P, from an incident power density S is characterized by a coupling cross section s, with units of area:

$$P = S \sigma$$

For frontdoor paths, σ is usually the effective area of an aperture, such as an antenna or slot.

The *Wunsch–Bell relation* for the power to induce failure is

$$P \sim \frac{1}{\sqrt{t}}$$

where t is the pulse duration, applicable between >100 nsec and <10 μsec.

TABLE A.11

Categories and Consequences of Electronic Effects

Failure Mode	Power Required	Wave Shape	Recovery Process	Recovery Time
Interference/ disturbance	Low	Repetitive pulse or continuous	Self-recovery	Seconds
Digital upset	Medium	Short pulse, single or repetitive	Operator intervention	Minutes
Damage	High	UWB or narrowband	Maintenance	Days

Power Beaming

The power–link parameter is

$$Z = \frac{D_t D_r}{\lambda R}$$

where D_t and D_r are the diameters of the transmitting and receiving antennas and R is the distance between the transmitter and receiver. For efficient transfer, the spot size must be ~D_r and $Z \geq 1$. An approximate analytic expression, good for $Z \sim 1$, is

$$\frac{P_r}{P_t} = 1 - e^{-Z^2}$$

Plasma Heating

Plasma heating resonant frequencies follow:

- *Ion cyclotron resonance heating* (ICRH)

$$f = f_{ci} = \frac{eB}{2\pi m_i}$$

- *Lower hybrid heating* (LHH)

$$f = f_{LH} \cong \frac{f_{pi}}{\left(1 - \frac{f_{pe}^2}{f_{ce}^2}\right)^{1/2}}$$

- *Electron cyclotron resonance heating* (ECRH)

$$f = f_{ce} = \frac{eB}{2\pi m_e}, \quad \text{or} \quad f = 2 f_{ce}$$

where m_i and m_e are the ion and electron masses, B is the magnitude of the local magnetic field, $f_{pe} = (n_e e^2/\varepsilon_0 m_e)^{1/2}/2$, with n_e the volume density of electrons and ε_0 the permittivity of vacuum, and $f_{pi} = (n_i Z_i^2 e^2/\varepsilon_0 m_i)^{1/2}/2$, with Z = 1 the charge state of the ions in the fusion plasma. At the densities and field values necessary for fusion, $f_{ci} \simeq 100$ MHz, $f_{LH} \simeq 5$ GHz, and $f_{ce} \simeq 140$ to 250 GHz.

Index

D

E

F

G

H

I

K

S

T

U

V

W

X